Discover Applied Sciences

Publishing model: **Open access**

Save journal View saved research

Explore open access funding Select institution

Journal menu

Search all Discover Applied Sciences articles →

Volume 8, Issue 5

May 2026

16 articles in this issue

Potential application of artificial intelligence in building information modeling: current state, challenges, and opportunities

Review | Open access | 10 March 2026 | Article: 489

Estimation of net primary productivity of vegetation based on spatio-temporal fusion algorithm of optical remote sensing images

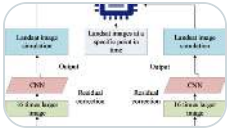

Research | Open access | 10 March 2026 | Article: 488

Human–Hamadryas baboon conflict in and around Simien Mountains National Park (SMNP), Ethiopia

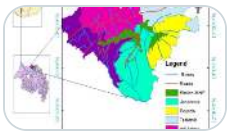

Research | Open access | 10 March 2026 | Article: 487

Investigating the influence of synthesis parameters on chitosan microparticle characteristics and Cr(VI) adsorption potential

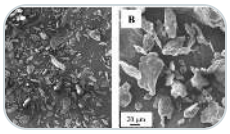

Research | Open access | 22 February 2026 | Article: 486

Geospatial modelling of landfill suitability using geophysical and remote sensing data in a basement complex area

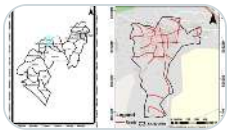

Research | Open access | 10 March 2026 | Article: 485

Japanese multimodal semantic understanding model based on transformer architecture and multi-task Bayesian federated learning

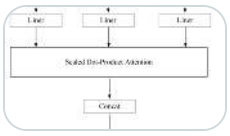

Research | Open access | 10 March 2026 | Article: 484

Three-dimensional finite element analysis of the impact of adjacent metro station construction on the structural response and safety of an existing tunnel

Research | Open access | 10 March 2026 | Article: 483

Dissipative double-diffusive mixed convective flow across a wavy vertical surface with activation energy and chemical reaction

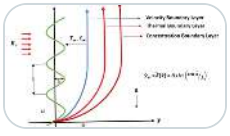

Research | Open access | 09 March 2026 | Article: 482

The role of plant microbiome engineering in stressful agriculture

Review | Open access | 09 March 2026 | Article: 481

Graph neural network-based remaining useful life prediction of milling tools using multi-sensor data

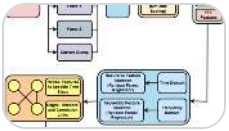

Research | Open access | 09 March 2026 | Article: 480

Application research on high speed railway roadbed deformation monitoring based on EM processing

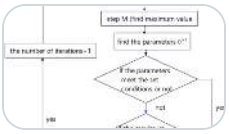

Research | Open access | 09 March 2026 | Article: 479

Effect of phytoremediated fly ash as soil amendment on morphological and biochemical traits of *Triticum aestivum*

Research | Open access | 09 March 2026 | Article: 478

Evaluating the impacts of land use/land cover change on soil moisture dynamics for sustainable water resources management in the Gojeb River sub-basin

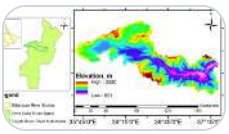

Research | Open access | 09 March 2026 | Article: 477

Refined identification of structural defects in compact GIS based on X-ray digital imaging distortion compensation

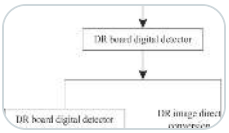

Research | Open access | 09 March 2026 | Article: 476

Mathematical analysis of a tumor suppression model incorporating vitamin intake

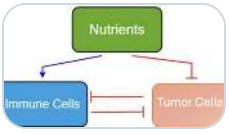

Research | Open access | 09 March 2026 | Article: 475

Optimization of grid-connected wind energy systems using DSTATCOM controlled by hybrid intelligent techniques

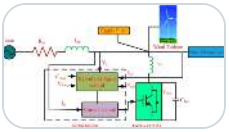

Research | Open access | 09 March 2026 | Article: 474

Discover Applied Sciences

RESEARCH Open Access

Investigating the influence of synthesis parameters on chitosan microparticle characteristics and Cr(VI) adsorption potential

Lanny Sapei[1,2*], Tokok Adiarto[3], Natalia Suseno[1], Nadhifatul Hidayah[1] and Nasira Kemhay[1]

*Correspondence:
Lanny Sapei
lanny.sapei@staff.ubaya.ac.id
[1]Department of Chemical Engineering, Faculty of Engineering, University of Surabaya, Raya Kalirungkut, Surabaya 60293, East Java, Indonesia
[2]Center of Excellence for Food Products and Health Supplements for Degenerative Conditions, University of Surabaya, Raya Kalirungkut, Surabaya 60293, East Java, Indonesia
[3]Department of Chemistry, University of Airlangga, Campus C Mulyorejo, Surabaya 60113, East Java, Indonesia

Abstract
Chitosan, a biopolymer derived from chitin, is a promising sustainable material for environmental remediation due to its biocompatibility and non-toxicity. Chitosan microparticles (ChMPs) offer enhanced functionality over bulk chitosan, yet their properties are highly sensitive to synthesis conditions. This study systematically evaluates the effects of bulk chitosan concentration (3, 6, and 9% w/v), degree of deacetylation (DD; 79.9%, 81.1%, and 82.6%), and stirring time (2, 4, and 6 h) on the morphology, size, and adsorption performance of ChMPs produced via ionic gelation followed by spray drying. SEM and FTIR analyses confirmed successful ionic cross-linking and revealed that longer stirring times and lower chitosan concentrations yielded smaller particles with more porous and irregular morphologies. Higher DD increased charge density and cross-linking intensity, resulting in structurally stable particles with enhanced surface accessibility. ChMPs synthesized under optimized conditions exhibited significantly improved Cr(VI) adsorption compared to bulk chitosan. These findings provide a reproducible framework for tailoring ChMP properties and demonstrate their potential as efficient, scalable, and sustainable adsorbents for heavy-metal removal.

Keywords Adsorption, Chitosan microparticles, Chromium(VI), Degree of deacetylation, Ionic gelation

1 Introduction

Chitosan is a linear polysaccharide composed of β-(1→4)-linked D-glucosamine and N-acetyl-D-glucosamine units derived from chitin, a structural polymer abundant in crustacean shells and fungal cell walls [5, 34]. Its backbone of glucopyranose units bearing amino groups ($-NH_2$) imparts a cationic nature under slightly acidic pH conditions [1, 30]. Chitosan is a gel- and film-forming polymer with the capacity to bind metal ions and organic compounds. It is also biodegradable, biocompatible, mucoadhesive, antimicrobial, and exhibits diverse bioactive properties [1, 9, 30, 33, 35, 42]. Recognizing these attributes, both the U.S. Food and Drug Administration (FDA) and the European Medicines Agency (EMA) have approved chitosan for clinical use in oral and parenteral

applications [46]. Consequently, chitosan is widely regarded as a versatile biopolymer with extensive applications in food, pharmaceuticals, healthcare, biomedicine, agriculture, and environmental remediation [1, 15, 26, 30, 39].

Chitosan nano- and microparticles have been extensively developed for the encapsulation and delivery of various drugs and bioactive compounds [10, 11, 15, 24, 27, 31, 44, 47]. They hold great promise as novel oral drug delivery systems with high efficacy, improved targeting ability, and potential applications in cancer therapy [27, 46]. Recently, chitosan microparticles (ChMPs) have been explored as carrier systems capable of delivering bioactive compounds to specific sites within the gastrointestinal tract, owing to their relatively larger particle size (> 300 nm), which prevents penetration across the extracellular space [11]. Beyond pharmaceutical applications, chitosan particles are considered excellent food-grade candidates for stabilizing Pickering emulsions, offering a natural and safe alternative to synthetic stabilizers [2, 39]. Furthermore, chitosan nano- and microparticles have been widely employed as efficient adsorbents for heavy metals and dyes, highlighting their potential role in environmental remediation [13, 28, 37, 49].

One of the most widely used techniques to produce chitosan nano- and microparticles is the crosslinking reaction via ionic (or ionotropic) gelation. This method is particularly attractive because it is simple, non-toxic, convenient, and does not require organic solvents, while also offering good controllability [33, 35, 43]. Among various crosslinkers, tripolyphosphate (TPP) is the most extensively employed due to its safety, biocompatibility, and multivalent properties. Unlike synthetic alternatives, polyphosphates such as TPP can hydrolyze into nutritionally beneficial simpler phosphates [3]. The resulting ionic gelation process is driven by electrostatic interactions between the positively charged amino groups of chitosan and the negatively charged phosphate groups of TPP under mechanical agitation. This interaction facilitates the formation of both inter- and intramolecular linkages [31], leading to the self-assembly of chitosan into spherical particles with tunable sizes and surface charges [11, 12, 44]. This crosslinking process is particularly advantageous due to its mild processing requirements, as it is carried out in an aqueous environment with low toxicity and simple conditions. Beyond its common use for encapsulating bioactive compounds, this method enables precise controllability of chitosan particle properties while avoiding undesirable side reactions [35, 44]. Such versatility is critical when engineering the surface architecture of micro-adsorbents for industrial wastewater treatment.

As a versatile industrial technique, spray drying offers a simple, continuous, and cost-effective route for converting liquid feed into powder with excellent flowability and stability [17]. The process involves atomizing the feed into fine droplets that are rapidly dried by hot air, producing spherical particles with precisely controlled size and morphology [38, 40]. While nanotechnology offers unique advantages, microparticles provide several practical benefits, particularly for adsorption purposes. Their larger size makes them more efficient and convenient in industrial settings, as they can be easily recovered using simple techniques such as filtration, sedimentation, or low-speed centrifugation. Moreover, microparticles reduce issues of clogging in membranes, filtration systems, or adsorption columns, making them more suitable for large-scale processes.

Heavy metals pose a significant threat to both the environment and human health due to their high toxicity, persistence, and non-degradable nature, causing organ damage even at low levels of exposure [7]. Humans and animals can be exposed to hexavalent

chromium, Cr(VI) through direct contact, ingestion of contaminated food and water, inhalation, or dermal absorption [19]. Potassium dichromate, a common source of Cr(VI), has historically been misused as a milk stabilizer to extend shelf life. However, its presence in food or drinking water presents severe health risks, including cancers of the prostate, stomach, kidney, urinary tract, and bones, as well as skin irritation, rhinitis, allergic contact dermatitis, gastrointestinal pain, and liver and kidney damage, even at trace levels [37, 41, 45].

Cr(VI), is a highly toxic pollutant released from diverse industrial activities, including metallurgy, leather tanning, and textile production [4, 28]. In the textile sector alone, Cr(VI) accounts for approximately 54% of dye effluents discharged into wastewater. Consequently, regulatory agencies have established a stringent maximum contaminant level of 0.05 mg/L for chromium in drinking water to mitigate its severe ecological and public health impacts [45]. Efficient wastewater management and potable water purification strategies are therefore paramount to support sustainable industrial development and public health risk reduction.

Chitosan nano- and microparticles have attracted considerable attention as adsorbents for heavy-metal remediation due to the high density of amino ($-NH_2$) and hydroxyl (–OH) functional groups that enable strong electrostatic and coordination interactions with metal ions. Their enhanced surface-area-to-volume ratio generally affords higher adsorption capacities than bulk chitosan [29, 37]. Among available treatment technologies, adsorption remains the most practical approach for Cr(VI) removal because of its cost-effectiveness and operational simplicity [26].

Despite these advantages, many reported chitosan-based adsorbents, particularly highly porous microspheres and chemically modified or magnetic derivatives, suffer from intrinsic limitations. Adsorption kinetics are often governed by slow intra-particle diffusion through complex internal pore networks [16, 37], while magnetic or chemically functionalized systems typically require multistep synthesis, specialized reagents, and external separation equipment [13, 22, 48, 50]. These factors limit scalability, process simplicity, and practical deployment.

To address these challenges, this study explores spray drying as a rapid, one-step route to fabricate chitosan microparticles (ChMPs) with highly textured, "brain-like" surface morphologies. The rapid solvent evaporation intrinsic to spray drying promotes surface wrinkling and dimple formation, maximizing active site accessibility while minimizing diffusion path lengths. This morphology enables efficient Cr(VI) sequestration without sacrificing microscale particle size, thereby facilitating straightforward post-adsorption recovery and offering a scalable alternative for practical water-treatment applications.

The formation and performance of chitosan nano- and microparticles are governed by multiple interdependent factors, including chitosan concentration, molecular weight, degree of deacetylation (DD), chitosan/TPP ratio, temperature, and hydrodynamic conditions [2, 3, 15, 24, 33, 42, 47]. While these parameters have been widely reported, most studies evaluate them in isolation or across broad compositional ranges, often overlooking subtle but critical interactions that arise within narrow processing windows.

In particular, the influence of DD is frequently treated as a secondary or categorical variable, despite its direct control over charge density, ionic cross-linking efficiency, and network shrinkage during drying. Systematic investigations probing small DD intervals, where minor changes can produce disproportionate effects on morphology, porosity,

and adsorption performance, remain scarce, especially for systems combining ionic gelation with spray drying. Furthermore, the coupled effects of DD with key process variables such as stirring time and bulk chitosan concentration have not been comprehensively resolved for this synthesis route.

The primary objective of this study was therefore to elucidate the combined influence of stirring time (2, 4, and 6 h), bulk chitosan concentration (3, 6, and 9% w/v), and narrowly spaced degrees of deacetylation (79.9%, 81.1%, and 82.6%) on the physicochemical characteristics of chitosan microparticles prepared via ionic gelation followed by spray drying. The resulting materials were systematically characterized by SEM and FTIR to resolve morphology, size, and cross-linking behavior, while Cr(VI) adsorption performance was employed as an indirect but functional probe of porosity and active-site accessibility.

Although chitosan-based adsorption has been extensively reported, the quantitative linkage between tightly controlled synthesis inputs and emergent microparticle structure remains insufficiently defined for reproducible, scalable production. By explicitly correlating narrow DD variations and processing conditions with structural and functional outcomes, this study establishes a mechanistic framework for tailoring chitosan microparticles with predictable performance. This structural–functional perspective provides essential technical guidance for the rational design of chitosan-based adsorbents in environmental bioremediation applications.

2 Materials and methods

2.1 Materials

Bulk chitosan derived from black shrimp shell with different degree of deacetylation (79.9%; 81.1%; and 82.6%) determined from FTIR spectra [43] were obtained from PT. Biotech Surindo, Indonesia. Other chemicals used were polysorbate/ Tween® 80 (Sigma Aldrich, Germany), acetic acid glacial 100% (Merck, Germany), potassium dichromate powder $K_2Cr_2O_7$ (Merck, Germany), Sodium tripolyphosphate powder, STPP (Merck, Germany).

2.2 Methods

2.2.1 Synthesis of chitosan microparticles

Bulk chitosan was obtained in different physical forms: flakes (DD = 79.9%), powder (DD = 81.1%), and semi-powder (DD = 82.6%). The flake and semi-powder types were ground using a blender (Miyako BL-102GS, Japan), and all chitosan powders were subsequently sieved through a 140-mesh screen to ensure uniform particle size. A 3% w/v bulk chitosan solution (DD = 81.1%) was prepared by dissolving 3 g of chitosan powder in 100 mL of 1% acetic acid solution under magnetic stirring at 300 rpm for 60 min. Subsequently, 25 mL of 0.2% (v/v) Tween 80 solution was added and stirred for 30 min prior to the dropwise addition of 10 mL of 0.1% (w/v) STPP solution. The mixture was then stirred for 2, 4, or 6 h at 300 rpm. The mixture was aged at room temperature for 5 days before spray drying. Spray drying was carried out using a BÜCHI B-290 mini spray dryer (Büchi Labortechnik AG, Switzerland), with approximately 150 mL of the chitosan solution at flow rate of 5 ml/min was atomized through a 0.7 mm two-fluid nozzle into the drying chamber. Hot air entered at 180 °C and aspiration rate of 100% while air pressure at nozzle was maintained at 1 bar. Experimental variations were performed sequentially:

first by varying stirring time, followed by bulk chitosan concentration (3%, 6%, and 9% w/v), and finally by chitosan DD (79.9%, 81.1%, and 82.6%).

2.2.2 Characterization of chitosan and chitosan microparticles

2.2.2.1 Determination of viscosity of bulk chitosan solution Bulk chitosan solution 1% w/v was prepared by dissolving 1 g of chitosan in 100 mL of 1% acetic acid solution. The viscosity of the solution was measured at room temperature using a Brookfield RVT viscometer (Brookfield, USA). Approximately 16 mL of the sample was transferred into the UL adapter chamber and sheared at 10 rpm. The dial reading was recorded after 30 s of measurement.

2.2.2.2 Determination of morphology and size of bulk chitosan and chitosan microparticles The morphology of chitosan microparticles was examined using scanning electron microscopy (SEM, FEI Inspect S50, FEI, USA). Samples were mounted on aluminum stubs with double-sided adhesive tape, sputter-coated with gold to improve conductivity, and analyzed at 20 kV with magnifications of 25,000×. The particle diameters were measured using digital image analysis based on the calibrated scale bars provided by the SEM instrumentation. To ensure representativeness, particles were selected from multiple micrographs at different locations. For comparison, the morphology of bulk chitosan powder (DD = 81.1%) was also analyzed by SEM (ThermoFisher Scientific™ Axia™ ChemiSEM™, USA) at 20 kV with magnifications of 100–500×.

2.2.2.3 Determination of chemical composition of bulk chitosan and chitosan microparticles The functional groups of bulk chitosan and chitosan microparticles were characterized by FTIR (IR-Tracer 100, Shimadzu, Japan). Samples were prepared as KBr pellets under dry conditions at 25 °C by thoroughly mixing 12.5 mg of sample with 250 mg of KBr and pressing the mixture at 10 tons using a hydraulic press (Specac, 15 Ton, England). Spectra were collected in the range of 4000–400 cm^{-1} with a resolution of 4 cm^{-1}, averaging 45 scans per sample.

2.2.2.4 Evaluation of adsorption performance of chitosan microparticles towards Cr(VI) ion Potassium dichromate ($K_2Cr_2O_7$) solution with the concentration of 50 ppm and initial pH of ~ 4 was prepared to simulate chromium-contaminated water. The adsorption capacity of chitosan microparticles was evaluated by monitoring the decrease in solution color intensity after adsorption and compared with bulk chitosan. Standard solutions of 10, 20, 30, 40, and 50 ppm were prepared to generate a calibration curve. The maximum absorption wavelength was determined by scanning the solutions between 300 and 600 nm using a UV–vis spectrophotometer (Lambda 950, PerkinElmer, USA), with the highest absorbance observed at 362 nm.

For the adsorption test, 25 mg of chitosan microparticles was dispersed into 30 mL of 50 ppm $K_2Cr_2O_7$ solution and stirred for 40 min with a magnetic stirrer. The mixture was then left undisturbed at room temperature for 24 h to allow equilibrium adsorption. Afterward, it was centrifuged (DSC-158, Digisystem, Taiwan) at 2500 rpm for 15 min. The supernatant (5 mL) was collected, and its absorbance at 362 nm was recorded using a UV–vis spectrophotometer (Lambda 950, PerkinElmer, USA). All analytical measurements were performed in duplicate to ensure instrumental precision, and the results are

Table 1 The properties of bulk chitosan

Bulk chitosan	Initial form	DD (%)	Viscosity (cP)
1	flake	79.9	39.64
2	powder	81.1	20.78
3	semi powder	82.6	70.33

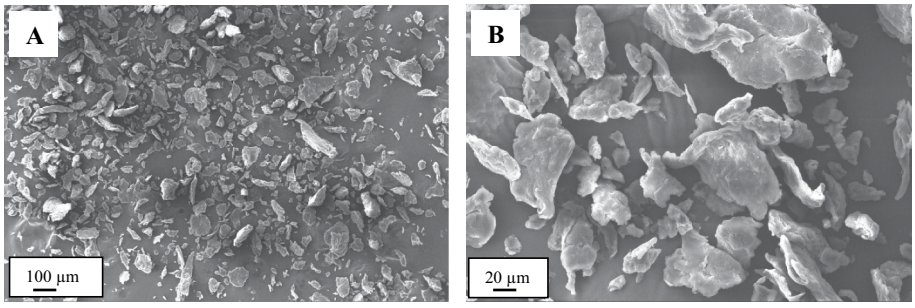

Fig. 1 SEM images of bulk chitosan (DD 81.1%) at different magnifications. **A** 100x; **B** 500x

presented as the mean values. The adsorption efficiency of $K_2Cr_2O_7$ by chitosan particles was calculated using Eq. (1):

$$\text{Adsorption efficiency } (\%) = \frac{(C_0 - C_{1)}}{C_0} x100\% \quad (1)$$

Whereas, C_0 is the initial concentration of $K_2Cr_2O_7$ solution and C_1 is the concentration after adsorption.

3 Results and discussion

3.1 Formation and physical characteristics of ChMPs

3.1.1 Properties of bulk chitosan

The characteristics of the produced ChMPs were strongly influenced by the properties of the bulk chitosan used as precursors (Table 1). Three types of bulk chitosan with different degrees of deacetylation (%DD) were employed. The viscosity of each bulk chitosan, which is positively correlated with its molecular weight, was determined. Chitosan with a DD of 81.1% exhibited the lowest viscosity (~ 20 cP), whereas that with a DD of 82.6% showed the highest viscosity (~ 70 cP), and the chitosan with a DD of 79.9% had an intermediate viscosity (~ 40 cP). All samples fell within the viscosity range of low molecular weight chitosan based on previous investigation [32]. Furthermore, according to the standard specification provided by Sigma-Aldrich (CAS No. 9012-76-4; product code 448869; batch BCCG9965), low-molecular-weight chitosan is characterised by a viscosity range of 20–300 cP. These findings indicated the distribution of molecular weights among the bulk chitosan samples.

SEM imaging of the bulk chitosan powder (Fig. 1) revealed large flake-like particles ranging from approximately 10 to 100 µm in size, with surfaces that appeared relatively smooth and showed minimal porosity.

3.1.2 Ionic gelation process

The synthesis of ChMPs was achieved through ionic gelation by mixing bulk chitosan with STPP. Initially, bulk chitosan was dissolved in 1% acetic acid, and then Tween 80,

a non-ionic surfactant, was added to improve polymer chain dispersion. This facilitated more uniform crosslinking in solution, enabling better control over particle size and morphology [33]. The addition of surfactant also enhanced suspension stability after nanoparticle formation [12] and coated the chitosan particles [21].

Upon the introduction of STPP, spontaneous electrostatic interactions occurred between the positively charged ammonium groups of chitosan and the negatively charged phosphate ions of STPP [11, 36]. In this mechanism, phosphate polyanions establish inter- and intramolecular linkages with chitosan amino groups [31]. STPP thus acts as a crosslinker, inducing chitosan chains to fold primarily through intramolecular interactions [36], leading to the formation of spherical particles. Gelation generates a three-dimensional network in which water becomes entrapped. Depending on process parameters, this ionic interaction can be tuned to produce particles ranging from the nano- to microscale [24, 42, 47].

3.1.3 Particle size and growth

The overall characteristics of the chitosan particles obtained from spray drying in this study are summarized in Table 2. The process predominantly yielded microparticles, categorized as entities larger than 100 nm. The formation of these micrometer-sized particles is highly dependent on the precursor concentration [24, 47]. In our study, the relatively high concentration of the chitosan solution likely shifted the viscous mixture into a semi-dilute regime. This state is characterized by significant polymer chain overlap, which, as suggested by Marsili's findings, enhances the probability of forming larger aggregates during the atomization and drying stages. Moreover, particle growth can result from the aggregation of smaller primary particles that tend to fuse into larger entities [36, 43].

3.1.4 Effect of aging and aggregation

The evolution of particle size over storage is not merely a physical enlargement but a complex structural rearrangement. This can be attributed to several factors, including aggregation that allows more efficient structural rearrangement and interactions between free polymer chains and the particle network, leading to the reorganization of intermolecular entanglements. In the presence of TPP, this process is further influenced by syneresis and swelling driven by osmotic water inflow ([36]; [43]). At room temperature, the increased kinetic energy promotes Brownian motion, which increases the frequency of particle collisions and further promotes size enlargement over time [43].

The aging process was strategically employed to optimize the feed properties for spray drying and to ensure the formation of micro-sized adsorbents. Particle growth and agglomeration were likely promoted during this aging process. The evolution of particle

Table 2 Estimated average particle size of ChMPs

Bulk chitosan (%DD)	[Chitosan solution] (%w/v)	Stirring time (h)	D_{avg} ChMPs (nm)
81.1	3	2	1565 ± 782
	3	4	1204 ± 432
	3	6	932 ± 580
	6	6	1000 ± 278
	9	6	1225 ± 860
79.9	9	6	850 ± 533
82.6	9	6	821 ± 614

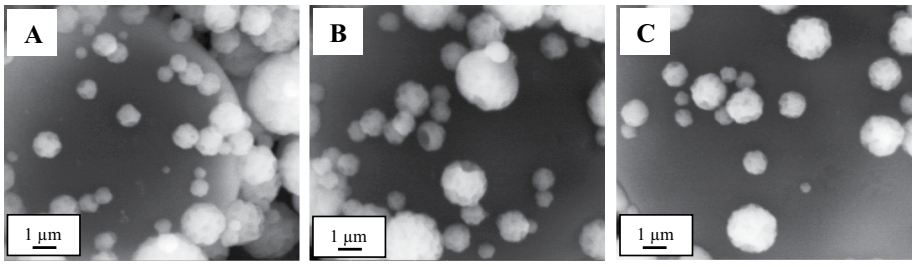

Fig. 2 SEM micrographs of ChMPs synthesized using 3% bulk chitosan (DD 81.1%) with different stirring time during STPP crosslinking. **A** 2 h; **B** 4 h; **C** 6 h. (Magnification: 25,000x)

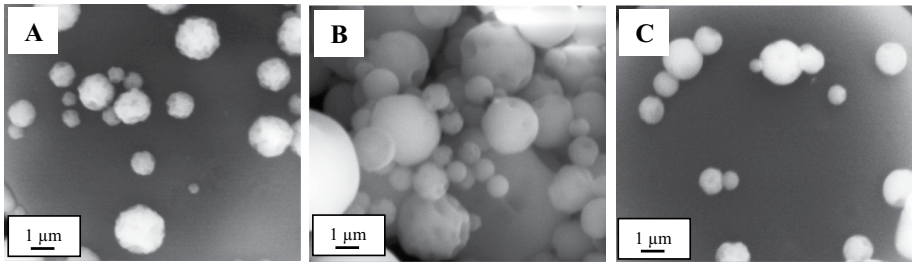

Fig. 3 SEM micrographs of ChMPs synthesized using bulk chitosan (DD 81.1%) under different concentrations with 6 h stirring during crosslinking. **A** 3%; **B** 6%; **C** 9%. (Magnification: 25,000x)

size over storage can be attributed to several factors, including aggregation that allows more efficient structural rearrangement, interactions between free polymer chains and the particle network leading to reorganization of intermolecular entanglements, as well as syneresis and swelling driven by the presence of TPP, which induces osmotic water inflow [36, 43].

From a process standpoint, this intentional aggregation is critical; without sufficient aging, the high viscosity of the chitosan solution would hinder atomization during the spray-drying process. Aggregation was particularly favored when the solution was left at room temperature, especially at higher chitosan concentrations, which enhanced particle rearrangement and led to the formation of larger aggregates [18, 36]. In addition, protonation of chitosan molecules contributed to molecular reorganization, while Brownian motion increased particle collisions, further promoting size enlargement over time [43].

This controlled enlargement to the micrometer scale is functionally beneficial, as it facilitates more efficient separation of the adsorbent from the aqueous phase via filtration or centrifugation after the adsorption process. While these mechanisms drive the formation of larger entities, the resulting microparticles maintain high site accessibility due to the textured surface morphology, thus balancing processability with adsorption performance.

3.1.5 Spray drying and porous structure development

Ultimately, spray drying of the mixtures resulted in the formation of micro-aggregated particles with porous structures, as observed in the SEM images (Figs. 2, 3 and 4). The formation of chitosan microparticles (ChMPs) occurs via ionic gelation between the positively charged protonated amino groups ($-NH_3^+$) of chitosan and the negatively charged

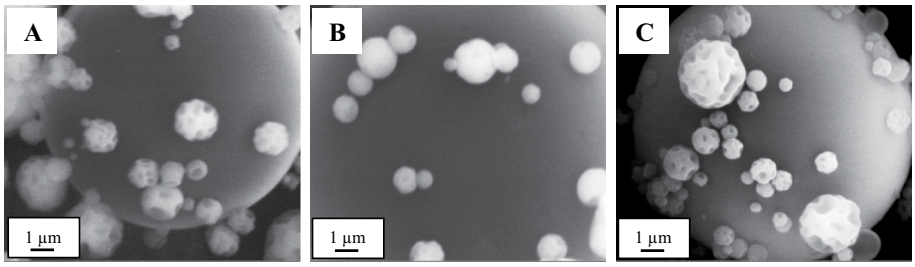

Fig. 4 SEM micrographs of ChMPs synthesized using 9% bulk chitosan at different DD values, stirred for 6 h during crosslinking. **A** 79.9%; **B** 81.1%; **C** 82.6%. (Magnification: 25,000x)

phosphate ions ($-P_3O_{10}^{5-}$) of TPP, leading to the development of a three-dimensional crosslinked network that stabilises the particles during the rapid spray-drying process.

Partial destabilisation of the ionic crosslinks between ammonium and phosphate ions may occur over time, creating interstitial voids within the aggregated structures and contributing to pore formation. During spray drying, these micro-aggregated structures are converted into dried powders, yielding spherical microparticles with highly porous morphologies. The porosity is further enhanced by the removal of water initially entrapped within the aggregates during atomisation and solvent evaporation in the spray-drying chamber.

Interestingly, surface dimples and a textured topography were observed across all samples, a characteristic feature of spray-dried particles. This morphology is attributed to the rapid solvent evaporation at 180 °C, which induces the formation of a solidified surface "skin" that subsequently collapses or wrinkles as the particle core shrinks during drying.

SEM analysis (Figs. 2, 3 and 4) indicates that the morphology of chitosan microparticles (ChMPs) is primarily dictated by chitosan concentration and degree of deacetylation (DD), rather than stirring time. As shown in Fig. 2, varying the stirring time (2–6 h) produced no significant morphological changes, indicating that ionic gelation occurs rapidly and reaches structural saturation early.

In contrast, Fig. 3 demonstrates that increasing chitosan concentration stabilises particle morphology. Higher solid content (9% w/v) resulted in less pronounced dimpling and wrinkling, as the more rigid matrix resisted collapse during solvent evaporation in spray drying.

Most pronounced morphological differences were observed with changes in DD (Fig. 4). Particles at 79% DD exhibited noticeable surface dimpling, 81% DD particles displayed a comparatively smoother and more homogeneous surface, while 82.6% DD particles showed a more irregular and dimpled morphology. The irregular surface of DD 79% may result from uneven ionic interactions due to the higher presence of residual acetyl groups, which hinder uniform gelation. The smoother morphology at 81% DD suggests a more homogeneous cross-linking network, where TPP ions are distributed uniformly within the chitosan matrix, leading to a stable and well-defined spherical structure. Furthermore, the markedly wrinkled surfaces observed at higher DD (82.6%) arise from increased charge density and stronger ionic cross-linking with TPP. During spray drying, this dense ionic network undergoes significant volumetric shrinkage, resulting in surface collapse and pronounced wrinkle formation.

The observed surface topographies are in good agreement with previous reports showing that spray drying commonly produces dimpled, hollow, or wrinkled particles [6, 8, 20, 23]. Kašpar et al. [20], reported a transition from brain-like structures at low cross-linking ratios to smoother surfaces at moderate cross-linking, followed by highly irregular morphologies at excessive cross-linking due to skin formation and buckling. Similar hollow and irregular particle morphologies were also described by Cerchiara et al. [8], and Khlibsuwan et al. [23], while Aranaz et al. [6], observed agglomerated brain-like structures in spray-dried chitosan systems.

Such highly porous and textured structures are particularly advantageous for adsorption applications, as they enhance the accessibility of active binding sites throughout the microparticle matrix.

3.2 Effect of bulk chitosan properties and process parameters

The characteristics of chitosan microparticles (ChMPs) are strongly influenced by both the intrinsic properties of the bulk chitosan (e.g. DD) and the synthesis conditions, including chitosan concentration and stirring time, as reported in previous studies by [2, 3, 27]. In this study, three key parameters, stirring time, bulk chitosan concentration, and DD were systematically evaluated for their effects on particle size and morphology, as discussed in Sects. 3.2.1, 3.2.2, 3.2.3.

3.2.1 Effect of stirring time

The impact of stirring duration on ChMP formation is quantitatively summarized in Table 2 and visually supported by Fig. 2. As the stirring time increased from 2 to 6 h, the average particle sizes exhibited a noticeable reduction from approximately 1500 nm to 900 nm. This trend suggests that longer stirring durations facilitate the mechanical separation of initial agglomerates into smaller, more discrete fragments through attrition, driven by continual particle collisions and shear forces within the mixing environment.

Despite this reduction, the ChMPs produced in this study remained within the microparticle range, as detailed in Table 2. This can be attributed to the relatively low stirring speed of 300 rpm used during ionic gelation. At this moderate intensity, localized concentration gradients likely persisted in the suspension, leading to non-uniform cross-linking between chitosan and TPP and the formation of larger entities. This is in contrast to studies employing higher energy inputs; for instance, stirring at 1200 rpm yielded nanoparticles of 299–377 nm [44], while high-speed homogenization at 3000 rpm combined with sonication produced highly stable particles < 200 nm [27]. Thus, the 300 rpm/6 h condition in this work was specifically chosen to maintain the micro-scale dimensions that facilitate easier post-adsorption recovery.

3.2.2 Effect of bulk chitosan concentration

An increase in bulk chitosan concentration resulted in larger ChMPs sizes. Particle size increased from ~ 932 nm at 3% w/v to ~ 1225 nm at 9% w/v (Table 2; Fig. 3). This agrees with previous reports showing that higher chitosan concentrations promote particle growth due to increased molecular proximity and crosslinking rates, which favor aggregate formation [2, 42]. Elevated chitosan concentration also raises solution viscosity, which may hinder diffusion and efficient interaction with the crosslinker (STPP), further promoting agglomeration and growth of micrometer-sized particles. Although Tween

80 was added as a surfactant to stabilize the suspension, its effect was not sufficient to prevent all agglomeration at higher concentrations.

An increase in bulk chitosan concentration also modifies the morphology of ChMPs. Higher concentrations lead to smoother particle surfaces due to increased viscosity, which enhances structural rigidity and resists collapse during spray drying, as discussed in the SEM analysis section.

3.2.3 Effect of degree of deacetylation (DD)

The average size of ChMPs generally decreased with increasing DD of bulk chitosan (Table 2; Fig. 4), consistent with prior findings [3]. Chitosan with higher DD contains more amine groups, which are protonated under acidic conditions and readily cross-linked with phosphate ions of STPP. This enhances electrostatic stabilisation, leading to smaller, more uniform particles. Notably, chitosan with 81.1% DD yielded the largest ChMPs among all samples. This behavior is likely associated with the lower viscosity of its bulk chitosan, indicative of reduced molecular weight and weaker chain entanglement, which favors particle growth. Moreover, the smoother surface morphology at this DD suggests a balanced cross-linking interaction that limits structural collapse during spray drying, resulting in the formation of larger and more stable particles. Conversely, the chitosan with 82.6% DD exhibited the highest viscosity, reflecting higher molecular weight and stronger intermolecular interactions, which hindered agglomeration and yielded smaller ChMPs [3]. Larger ChMPs prepared from higher molecular weight chitosan also exhibit stronger intermolecular entanglements and more extensive hydrogen bonding, producing a stable gel network that resists size changes during synthesis [36]. Nevertheless, previous reports indicate that DD alone may exert limited control over particle formation [42]. DD may dictate the morphology of ChMPs, as evidenced by Fig. 4, where all particles are spherical with porous or dimpled surfaces, while those derived from 81.1% DD chitosan exhibit comparatively smoother and less porous morphologies.

Overall, the results demonstrate that both the intrinsic properties of bulk chitosan and the applied process conditions significantly influence ChMPs characteristics. Stirring time primarily affected particle fragmentation, whereas bulk chitosan concentration strongly governed particle growth, aggregation, and morphology. The degree of deacetylation (DD) had a pronounced effect on the development of brain-like surface morphologies, as discussed in the SEM analysis section.

3.3 FTIR analysis of chitosan and ChMPs

The FTIR spectra of bulk chitosan and ChMPs are shown in Fig. 5. A broad band between 3700 and 3300 cm^{-1} was attributed to overlapping O–H and N–H stretching vibrations in the chitosan matrix [9, 35, 36]. In ChMPs, this band appeared narrower and sharper, suggesting a weakening of hydrogen bonding interactions. In bulk chitosan, strong intermolecular hydrogen bonds dominate, whereas in ChMPs, these interactions are partially replaced by ionic interactions between protonated amine groups ($–NH_3^+$) and phosphate ions from STPP during crosslinking.

Both bulk chitosan and ChMPs exhibited doublet peaks around 2900 cm^{-1} corresponding to C–H stretching. Notably, the N–H vibrational modes were shifted to lower frequencies upon crosslinking. The N–H bending band shifted from 1651 to 1640 cm^{-1}, while the N–H stretching band shifted from 1597 to 1559 cm^{-1}, confirming ionic

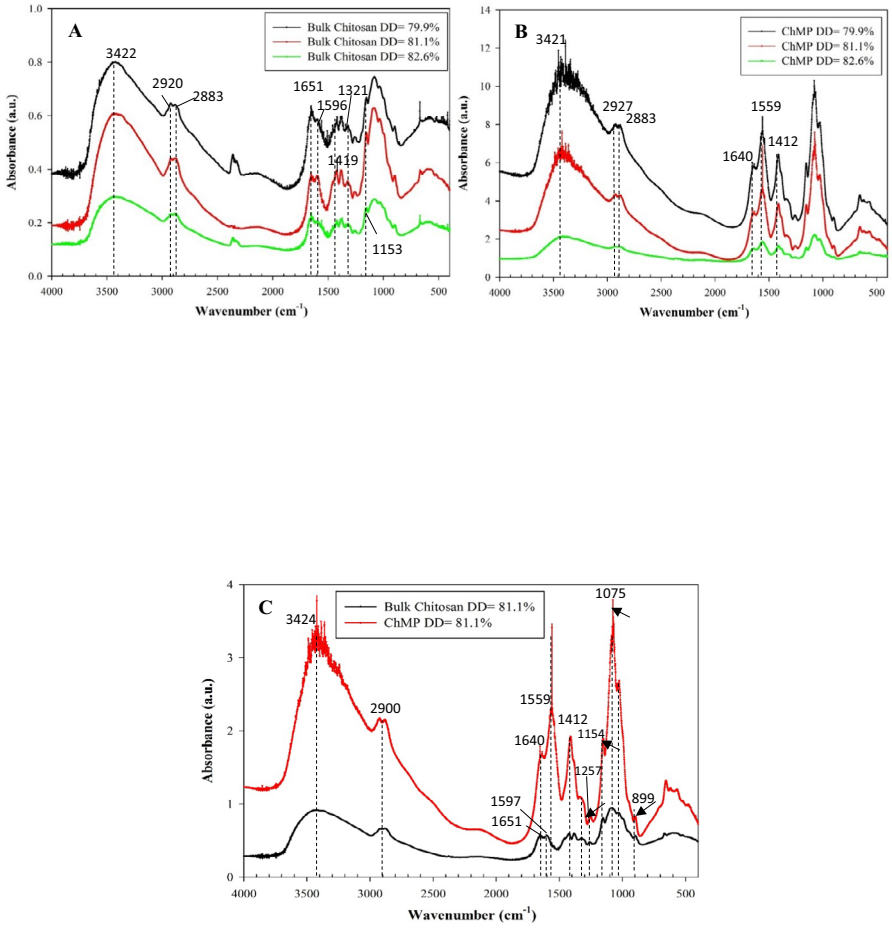

Fig. 5 FTIR spectra. **A** Bulk Chitosan with different DD; **B** ChMP with different DD; **C** Bulk Chitosan and ChMP with DD 81.1%. The arrow indicates phosphate-related vibrations

complexation between chitosan ammonium ions and phosphate groups [9, 35]. In addition, the CH_2 deformation band at 1412 cm^{-1} became more intense, reflecting increased polarization of the carbonyl group after crosslinking [9].

In the bulk chitosan spectrum, bands at ~ 1321 cm^{-1} and 1153 cm^{-1} were assigned to amide type I C–N stretching and asymmetric C–O–C stretching, respectively. In contrast, the ChMP spectra showed distinct phosphate-related vibrations, with peaks at 1257, 1154, and 1075 cm^{-1} corresponding to P = O, PO_2, and PO_3 stretching, respectively, along with an antisymmetric P–O–P stretching band at 899 cm^{-1} [9]. These new absorption bands provide clear evidence of STPP crosslinking within the ChMP structure.

3.4 Adsorption efficiency of chitosan microparticles towards Cr(VI) ion

The adsorption test of Cr(VI) ions was carried out by dispersing ChMPs into $K_2Cr_2O_7$ solution as a simple evaluation of their performance and potential applications. Adsorption was primarily facilitated by hydroxyl (–OH) and amine ($–NH_2$) groups present in the chitosan microparticles [28, 37, 50]. At acidic pH, these groups become protonated: amines yield ammonium ions ($–NH_3^+$), while hydroxyl groups form $–OH_2^+$ [13, 25]. At pH ~ 4, Cr(VI) exists mainly as $HCrO_4^-$, enabling strong electrostatic attraction between negatively charged chromate anions and the positively charged chitosan surface [25].

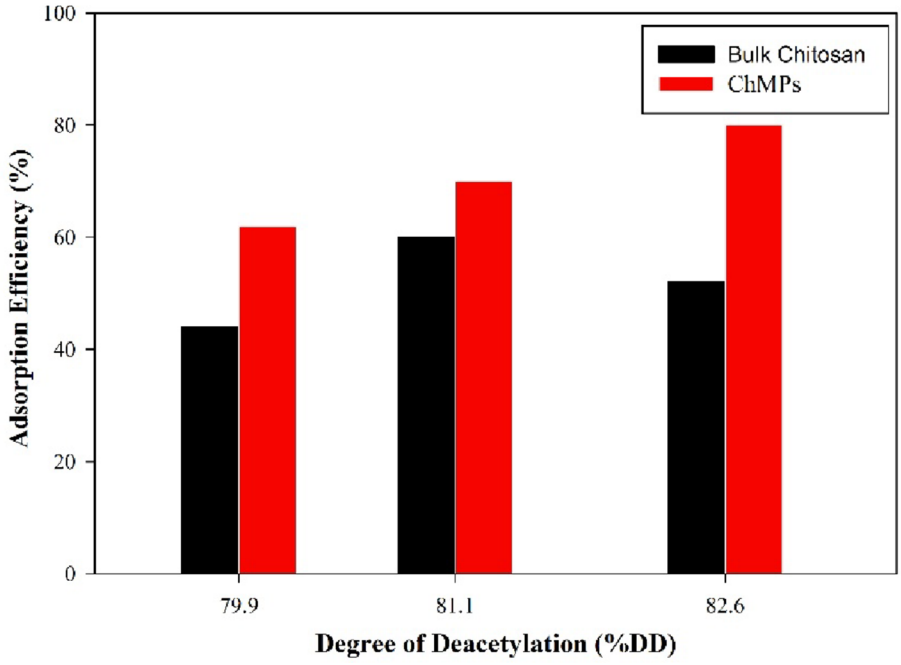

Fig. 6 Adsorption efficiency of bulk chitosan and ChMPs with different DD values toward Cr(VI) ion. (Note: the data represents the mean of duplicate measurements with a Relative Standard Deviation (RSD) < 0.5%)

Thus, the binding mechanism is dominated by physical electrostatic interactions rather than chemisorption [26]. In addition, partial reduction of Cr(VI) to the less toxic Cr(III) may also occur, as chromate anions oxidize reactive groups on the sorbent surface [13].

The smaller particle size and porous structure of ChMPs compared to bulk chitosan enhanced the accessibility of functional groups, thereby facilitating the adsorption process. The internal pores and cavities created within aggregated ChMPs allowed not only surface adsorption but also entrapment of Cr(VI) ions within the porous matrix, preventing desorption and enhancing binding stability. As shown in Fig. 6, ChMPs exhibited higher adsorption efficiency than bulk chitosan. Beyond better performance, the microparticles could also be more easily separated from suspension after adsorption, an advantage for practical applications.

Microparticles derived from high-viscosity, high-molecular-weight chitosan formed more coherent internal networks that, upon drying, developed into porous structures conducive to adsorbate diffusion. An increased degree of deacetylation (DD) further enhanced adsorption performance. Although a portion of amine groups was consumed during ionic cross-linking with TPP, chitosan with higher DD retained a greater number of free amine groups that, upon protonation, provided additional binding sites for Cr(VI). The resulting higher positive charge density strengthened electrostatic interactions and improved microparticle stability.

It turned out that the enhanced adsorption observed at 81% DD is primarily driven by chemical functionality rather than surface morphology. Despite exhibiting smoother and less porous surfaces than the 79% DD samples, the 81% DD ChMPs showed significantly higher Cr(VI) adsorption, confirming that adsorption efficiency is mainly governed by the density of protonated amine groups ($-NH_3^+$). At higher DD, increased surface irregularity and wrinkling further enhanced adsorption by increasing the surface-to-volume ratio and improving access to active binding sites.

Overall adsorption efficiency was strongly dependent on the properties of the precursor chitosan. ChMPs prepared from 82.6% DD chitosan exhibited the greatest enhancement, achieving up to 35% higher adsorption compared to bulk chitosan, while 79% DD samples showed an intermediate improvement of approximately 30%. In contrast, ChMPs derived from 81.1% DD chitosan displayed only a ~ 15% increase, which can be attributed to their smoother, less porous morphology (Fig. 4) and lower viscosity. These features promoted particle agglomeration into larger, irregular structures (Table 2), reducing accessibility to internal active sites and trapping functional groups within the particle interior.

In this study, the adsorption capacity of the prepared ChMPs ranged from 26 to 48 mg/g at an adsorbent dose of 0.83 g/L. This performance is comparable to that of conventional chitosan microspheres, which exhibited an adsorption capacity of 39.11 mg/g [16]. Significantly higher adsorption capacities of 704.44 mg/g, have been reported for highly engineered or modified chitosan-based systems, such as highly porous frozen chitosan microspheres [37] and modified magnetic chitosan adsorbents, which achieved 153.85 mg/g at pH 4 for 0.5 g/L dose [50], 78 mg/ g at pH 5 for 0.5 g/L dose [13], 299.50 mg/g under visible light irradiation [48], and 188.68 mg/g at pH 5 [22].

It should be noted that these higher adsorption capacities were generally obtained under optimized conditions, including lower adsorbent dosages, controlled pH environments, additional functionalization, or external energy input (e.g., light irradiation). In contrast, the present study employed a simple ionic gelation–spray drying approach without chemical modification, highlighting that the achieved adsorption capacity is competitive for a non-modified, scalable, and environmentally benign system.

Collectively, these results indicate that optimal Cr(VI) adsorption is governed by a synergy between chemical charge density and particle morphology. Higher DD enhanced the density of protonated amine groups, while porous and irregular ("brain-like") surfaces increased active-site accessibility, together maximizing adsorption efficiency. The broad particle size distribution observed is advantageous for Cr(VI) removal: submicron particles provide high surface area for rapid adsorption kinetics, whereas larger microparticles allow facile recovery by conventional filtration.

Overall, the porous ChMPs clearly outperformed bulk chitosan, highlighting their potential as effective adsorbents for heavy metal remediation. Although their adsorption capacity (25–50 mg g^{-1}) is lower than that of some chemically modified magnetic chitosan systems (up to ~ 300 mg g^{-1}), this study emphasizes process efficiency and scalability. Unlike magnetic adsorbents requiring complex functionalization and external separation, these ChMPs are produced via a rapid, one-step spray-drying process. Their brain-like morphology ensures high site accessibility, while their micrometer-scale size enables straightforward recovery, making them a cost-effective and practical candidate for industrial Cr(VI) removal.

4 Conclusion

This work establishes a robust and reproducible strategy for producing chitosan microparticles (ChMPs) via ionic gelation with STPP and elucidates the direct relationship between synthesis parameters, morphology, and Cr(VI) adsorption performance. FTIR analysis confirmed stable ionic cross-linking between chitosan ammonium groups and STPP phosphate groups, validating the structural integrity of the ChMP framework.

Beyond confirming known processing trends, this study provides new mechanistic insight into the dominant role of degree of deacetylation (DD) in governing particle stability and adsorption efficiency. A higher DD (82.6%) supplied sufficient charge density to promote strong ionic cross-linking, suppress particle agglomeration, and preserve a highly porous architecture. Controlled stirring time (6 h) was identified as a critical threshold for achieving porous, micro-aggregated structures that maximize the accessibility of protonated amine sites ($–NH_3^+$), which are central to Cr(VI) sequestration.

Morphological analysis revealed that adsorption performance is governed by a synergy between chemical functionality and particle architecture. While smoother particles at intermediate DD (81.1%) exhibited enhanced chemical activity, their reduced porosity limited overall adsorption gains. In contrast, highly porous and irregular morphologies at elevated DD combined high surface-to-volume ratios with increased charge density, yielding superior Cr(VI) uptake.

By explicitly linking bulk chitosan properties, process control, and functional performance, this work delivers a scalable design framework for chitosan-based adsorbents. The one-step spray-drying approach offers a practical alternative to chemically modified systems, balancing adsorption efficiency with operational simplicity. These findings advance the rational engineering of biopolymer adsorbents and support the translation of ChMPs from laboratory studies to predictable, large-scale applications in water remediation.

Acknowledgements
We thank Ms. Dyah Ayu Ambarsari and Mr. Arief Rahman Hakim for the technical assistance during the experiments. Financial support from the Directorate of Research and Community Service (DPPM), Ministry of Higher Education, Science, and Technology of the Republic of Indonesia, through the Center of Excellence for Food Products and Health Supplements for Degenerative Conditions (second-year grant), under Contract No. 029/C3/DT.05.00/PL-PUIPT LANJUTAN/2026 is gratefully acknowledged.

Author contributions
L.S. : writing-review & editing, validation, supervision, resources, funding acquisition, formal analysis, data curation; T.A.: conceptualization, methodology, supervision, resources; N.S.: methodology, data curation, resources; N.H.: writing-original draft, methodology, investigation, formal analysis, data curation; N.K.: writing-original draft, methodology, investigation, formal analysis, data curation.

Data availability
The datasets generated during and/or analysed during the current study are available from the corresponding author on reasonable request.

Declarations

Ethics approval and consent to particpate
Not applicable.

Consent for publication
Not applicable.

Competing interests
The authors declare no competing interests.

Received: 22 November 2025 / Accepted: 19 February 2026
Published online: 22 February 2026

References

1. Adeyemi AO, Ojoawo SO. Production and characterization of chitosan of crustacean shells. Mater Today: Proc. 2023;88:128–34. https://doi.org/10.1016/J.MATPR.2023.05.729.
2. Alehosseini E, Tabarestani S, Kharazmi H, Alehosseini E, Tabarestani HS, Kharazmi MS, Jafari SM. Physicochemical, Thermal, and Morphological Properties of Chitosan Nanoparticles Produced by Ionic Gelation. Foods 2022. 2022;11(23):3841. https://doi.org/10.3390/FOODS11233841. *11*.
3. Al-Nemrawi NK, Alsharif SSM, Dave RH. (2018). *PREPARATION OF CHITOSAN-TPP NANOPARTICLES: THE INFLUENCE OF CHITOSAN POLYMERIC PROPERTIES AND FORMULATION VARIABLES*. https://doi.org/10.22159/ijap.2018v10i5.26375

4. Al-Qarni A, Al-Balawi MM, Al-Qarni I, Rashad M. High performance adsorption efficiency of metal oxides towards potassium dichromate. Desalination Water Treat. 2024;319:100506. https://doi.org/10.1016/J.DWT.2024.100506.
5. Amor I, Ben, Zeghoud S, Hemmami H, Ahmed S. Polysaccharides: Chitin and Chitosan. Chitn Chitosan: Phys Chem Prop. 2025;1–32. https://doi.org/10.1201/9781003589778-1.
6. Aranaz I, Paños I, Peniche C, Heras Á, Acosta N. (n.d.). *molecules Chitosan Spray-Dried Microparticles for Controlled Delivery of Venlafaxine Hydrochloride*. https://doi.org/10.3390/molecules22111980
7. Briffa J, Sinagra E, Blundell R. (2020). Heavy metal pollution in the environment and their toxicological effects on humans. *Heliyon*, *6*(9), e04691. https://doi.org/10.1016/J.HELIYON.2020.E04691/ASSET/D0EBFF86-7520-4BB6-87F1-F13F95A83B0C/MAIN.ASSETS/GR7.JPG
8. Cerchiara T, Abruzzo A, Di Cagno M, Bigucci F, Bauer-Brandl A, Parolin C, Vitali B, Gallucci MC, Luppi B. Chitosan based micro- and nanoparticles for colon-targeted delivery of vancomycin prepared by alternative processing methods. Eur J Pharm Biopharm. 2015;92:112–9. https://doi.org/10.1016/J.EJPB.2015.03.004.
9. de Carvalho FG, Magalhães TC, Teixeira NM, Gondim BLC, Carlo HL, dos Santos RL, de Oliveira AR, Denadai ÂML. Synthesis and characterization of TPP/chitosan nanoparticles: Colloidal mechanism of reaction and antifungal effect on C. albicans biofilm formation. Mater Sci Engineering: C. 2019;104:109885. https://doi.org/10.1016/J.MSEC.2019.109885.
10. Di Santo MC, Antoni D', Domínguez CL, Rubio AP, Alaimo A, Pérez OE. Chitosan-tripolyphosphate nanoparticles designed to encapsulate polyphenolic compounds for biomedical and pharmaceutical applications – A review. Biomed Pharmacother. 2021;142:111970. https://doi.org/10.1016/J.BIOPHA.2021.111970.
11. Espinosa-Andrews H, Barbosa-Nuñez JA, Martínez-Velázquez M, Castillo-Herrera GA, Haro-González JN. Effects of phosphate salts and ultrasonication on the formation and characteristics of phosphate-chitosan microparticles. Food Phys. 2024;1:100023. https://doi.org/10.1016/J.FOODP.2024.100023.
12. Gutiérrez-Ruíz SC, Cortes H, González-Torres M, Almarhoon ZM, Gürer ES, Sharifi-Rad J, Leyva-Gómez G. Optimize the parameters for the synthesis by the ionic gelation technique, purification, and freeze-drying of chitosan-sodium tripolyphosphate nanoparticles for biomedical purposes. J Biol Eng. 2024;18(1):1–16. https://doi.org/10.1186/S13036-024-00403-W/FIGURES/7.
13. Hamza MF, Hamad DM, Hamad NA, Abdel-Rahman AAH, Fouda A, Wei Y, Guibal E, El-Etrawy AAS. Functionalization of magnetic chitosan microparticles for high-performance removal of chromate from aqueous solutions and tannery effluent. Chem Eng J. 2022;428:131775. https://doi.org/10.1016/J.CEJ.2021.131775.
14. Hejjaji EMA, Smith AM, Morris GA. The potential of chitosan-tripolyphosphate microparticles in the visualisation of latent fingermarks. Food Hydrocolloids. 2017;71:290–8. https://doi.org/10.1016/J.FOODHYD.2016.12.020.
15. Hoang NH, Thanh T, Le, Sangpueak R, Treekoon J, Saengchan C, Thepbandit W, Papathoti NK, Kamkaew A, Buensanteai N. Chitosan Nanoparticles-Based Ionic Gelation Method: A Promising Candidate for Plant Disease Management. Polym 2022. 2022;14(4):662. https://doi.org/10.3390/POLYM14040662. *14*.
16. Hua C, Zhang R, Bai F, Lu P, Liang X. Removal of chromium (VI) from aqueous solutions using quaternized chitosan microspheres. Chin J Chem Eng. 2017;25(2):153–8. https://doi.org/10.1016/J.CJCHE.2016.08.024.
17. Jafari SM, Samborska K. Spray drying for the retention of food bioactive compounds and nutraceuticals–150th anniversary of spray drying. Drying Technol. 2021;39(12):1773. https://doi.org/10.1080/07373937.2021.1972521. ;CSUBTYPE:STRING:SPECIAL;PAGE:STRING:ARTICLE/CHAPTER.
18. Jonassen H, Kjøniksen AL, Hiorth M. Stability of chitosan nanoparticles cross-linked with tripolyphosphate. Biomacromolecules. 2012;13(11):3747–56. https://doi.org/10.1021/BM301207A/SUPPL_FILE/BM301207A_SI_001.PDF.
19. Jyothi NR. Heavy Metal Sources and Their Effects on Human Health. Heavy Met - Their Environ Impacts Mitigation. 2020. https://doi.org/10.5772/INTECHOPEN.95370.
20. Kašpar O, Jakubec M, Štěpánek F. Characterization of spray dried chitosan–TPP microparticles formed by two- and three-fluid nozzles. Powder Technol. 2013;240:31–40. https://doi.org/10.1016/J.POWTEC.2012.07.010.
21. Kaur H, Ghosh S, Kumar P, Basu B, Nagpal K. Ellagic acid-loaded, tween 80-coated, chitosan nanoparticles as a promising therapeutic approach against breast cancer: In-vitro and in-vivo study. Life Sci. 2021;284:119927. https://doi.org/10.1016/J.LFS.2021.119927.
22. Khalil TE, Abdel-Salam AH, Mohamed LA, El-Meligy E, El-Dissouky A. Crosslinked modified chitosan biopolymer for enhanced removal of toxic Cr(VI) from aqueous solution. Int J Biol Macromol. 2023;234:123719. https://doi.org/10.1016/J.IJBIOMAC.2023.123719.
23. Khlibsuwan R, Siepmann F, Siepmann J, Pongjanyakul T. Chitosan-clay nanocomposite microparticles for controlled drug delivery: Effects of the MAS content and TPP crosslinking. J Drug Deliv Sci Technol. 2017;40:1–10. https://doi.org/10.1016/J.JDDST.2017.05.012.
24. Marsili L, Dal Bo M, Berti F, Toffoli G. Thermoresponsive Chitosan-Grafted-Poly(N-vinylcaprolactam) Microgels via Ionotropic Gelation for Oncological Applications. Pharm 2021. 2021;13(10):1654. https://doi.org/10.3390/PHARMACEUTICS13101654. *13*.
25. Mishima K, Du X, Sekiguchi S, Kano N. Experimental and Theoretical Studies on the Adsorption and Desorption Mechanisms of Chromate Ions on Cross-Linked Chitosan. J Funct Biomaterials 2017. 2017;8(4):51. https://doi.org/10.3390/JFB8040051. *8*.
26. Moussout H, Ahlafi H, Aazza M, Akili E, C. Performances of local chitosan and its nanocomposite 5%Bentonite/Chitosan in the removal of chromium ions (Cr(VI)) from wastewater. Int J Biol Macromol. 2018;108:1063–73. https://doi.org/10.1016/J.IJBIOMAC.2017.11.018.
27. Muchtaromah B, Minarno EB, Annisa R, Ansori ANM, Fajriyah EN, Fitriasari PD, Suhargo L, Mishima K. Synthesis and Optimization of Nanoparticle Chitosan-Tripolyphospate Centella asiatica using Ionic Gelation Method with Difference Sonification Time. Res J Pharm Technol. 2023;16(8):3847–51. https://doi.org/10.52711/0974-360X.2023.00635.
28. Muddin NAI, Badsha MM, Arafath MA, Merican ZMA, Hossain MS. Magnetic chitosan nanoparticles as a potential biosorbent for the removal of Cr(VI) from wastewater: Synthesis, environmental impact and challenges. Desalination Water Treat. 2024a;319:100449. https://doi.org/10.1016/J.DWT.2024.100449.
29. Muddin NAI, Badsha MM, Arafath MA, Merican ZMA, Hossain MS. Magnetic chitosan nanoparticles as a potential biosorbent for the removal of Cr(VI) from wastewater: Synthesis, environmental impact and challenges. Desalination Water Treat. 2024b;319:100449. https://doi.org/10.1016/J.DWT.2024.100449.

30. Muthu M, Gopal J, Chun S, Devadoss AJP, Hasan N, Sivanesan I. (2021). Crustacean Waste-Derived Chitosan: Antioxidant Properties and Future Perspective. *Antioxidants 2021, Vol. 10, Page 228, 10*(2), 228. https://doi.org/10.3390/ANTIOX10020228
31. Nair RS, Morris A, Billa N, Leong CO. An Evaluation of Curcumin-Encapsulated Chitosan Nanoparticles for Transdermal Delivery. AAPS PharmSciTech. 2019;20(2):1–13. https://doi.org/10.1208/S12249-018-1279-6/METRICS.
32. Ngan LTK, Wang SL, Hiep IM, Luong PM, Vui NT, Crossed D, Signinh TM, Dzung NA. Preparation of chitosan nanoparticles by spray drying, and their antibacterial activity. Res Chem Intermediates 2014. 2014;40:6(6):2165–75. https://doi.org/10.1007/S11164-014-1594-9. *40*.
33. Pan C, Qian J, Fan J, Guo H, Gou L, Yang H, Liang C. Preparation nanoparticle by ionic cross-linked emulsified chitosan and its antibacterial activity. Colloids Surf A. 2019;568:362–70. https://doi.org/10.1016/J.COLSURFA.2019.02.039.
34. Pellis A, Guebitz GM, Nyanhongo GS. Chitosan: Sources, Processing and Modification Techniques. Gels 2022. 2022;8(7). https://doi.org/10.3390/GELS8070393. *8*.
35. Popova EV, Zorin IM, Domnina NS, Novikova II, Krasnobaeva IL. Chitosan–Tripolyphosphate Nanoparticles: Synthesis by the Ionic Gelation Method, Properties, and Biological Activity. Russ J Gen Chem. 2020;90(7):1304–11. https://doi.org/10.1134/S1070363220070178/METRICS.
36. Rampino A, Borgogna M, Blasi P, Bellich B, Cesàro A. Chitosan nanoparticles: Preparation, size evolution and stability. Int J Pharm. 2013;455(1–2):219–28. https://doi.org/10.1016/J.IJPHARM.2013.07.034.
37. Ren L, Xu J, Zhang Y, Zhou J, Chen D, Chang Z. Preparation and characterization of porous chitosan microspheres and adsorption performance for hexavalent chromium. Int J Biol Macromol. 2019;135:898–906. https://doi.org/10.1016/J.IJBIOMAC.2019.06.007.
38. Sánchez-Osorno DM, López-Jaramillo MC, Paz C, Villa AV, Peresin AL, M. S., Martínez-Galán JP. Recent Advances in the Microencapsulation of Essential Oils, Lipids, and Compound Lipids through Spray Drying: A Review. Pharm 2023. 2023;15(5):1490. https://doi.org/10.3390/PHARMACEUTICS15051490. *15*.
39. Sapei L, Agustriyanto R, Fitriani EW, Levy Z, Sumampouw C. Enhancement of the Stability of W/O/W Double Emulsion by Chitosan Modified Rice Husk Silica. Int J Technol. 2022;13(3):584–95. https://doi.org/10.14716/IJTECH.V13I3.4752.
40. Sapei L, Mustika PCBW, Sutrisna PD, Agustriyanto R, Setyopratomo P, Santoso GV, Utama JP, Indrawanto R. Inulin-coated Virgin Coconut Oil (VCO) powder produced by spray drying. Appl Food Res. 2025;5(1):100721. https://doi.org/10.1016/J.AFRES.2025.100721.
41. Sharma P, Nangare S, Tade R, Patil P, Bari S, Patil D. (2024). *Potassium Dichromate Detection: Carbon Quantum Dot-based Fluorescent Turn-Off Nanoprobe Design*. https://doi.org/10.26599/NBE.2024.9290069
42. Sreekumar S, Goycoolea FM, Moerschbacher BM, Rivera-Rodriguez GR. Parameters influencing the size of chitosan-TPP nano- and microparticles. Sci Rep 2018. 2018;8:1(1):1–11. https://doi.org/10.1038/s41598-018-23064-4. *8*.
43. Tsai ML, Chen RH, Bai SW, Chen WY. The storage stability of chitosan/tripolyphosphate nanoparticles in a phosphate buffer. Carbohydr Polym. 2011;84(2):756–61. https://doi.org/10.1016/J.CARBPOL.2010.04.040.
44. Upadhyay J, Shah K, Lalbhai SN. Implementation of factorial experimental design in chitosan-tripolyphosphate nanoparticles development by ionotropic gelation. Int J Health Sci. 2022;6(S4):8529–43. https://doi.org/10.53730/ijhs.v6nS4.10613.
45. Velusamy S, Roy A, Sundaram S, Kumar Mallick T. A Review on Heavy Metal Ions and Containing Dyes Removal Through Graphene Oxide-Based Adsorption Strategies for Textile Wastewater Treatment. Chem Record. 2021;21(7):1570–610. https://doi.org/10.1002/TCR.202000153.
46. Wang Y, Li P, Tran TTD, Zhang J, Kong L. Manufacturing Techniques and Surface Engineering of Polymer Based Nanoparticles for Targeted Drug Delivery to Cancer. Nanomaterials 2016. 2016;6(2):26. https://doi.org/10.3390/NANO6020026. *6*.
47. Weyers M, Peterson B, Hamman JH, Steenekamp JH. Formulation of Chitosan Microparticles for Enhanced Intranasal Macromolecular Compound Delivery: Factors That Influence Particle Size during Ionic Gelation. Gels 2022. 2022;8(11):686. https://doi.org/10.3390/GELS8110686. *8*.
48. Zahra MH, Hamza MF, El-Habibi G, Abdel-Rahman AAH, Mira HI, Wei Y, Alotaibi SH, Amer HH, Goda AES, Hamad NA. Synthesis of a Novel Adsorbent Based on Chitosan Magnetite Nanoparticles for the High Sorption of Cr (VI) Ions: A Study of Photocatalysis and Recovery on Tannery Effluents. Catalysts 2022. 2022;12(7). https://doi.org/10.3390/CATAL12070678. *12*.
49. Zhai L, Bai Z, Zhu Y, Wang B, Luo W. Fabrication of chitosan microspheres for efficient adsorption of methyl orange. Chin J Chem Eng. 2018;26(3):657–66. https://doi.org/10.1016/J.CJCHE.2017.08.015.
50. Zheng C, Zheng H, Wang Y, Wang Y, Qu W, An Q, Liu Y. Synthesis of novel modified magnetic chitosan particles and their adsorption performance toward Cr(VI). Bioresour Technol. 2018;267:1–8. https://doi.org/10.1016/J.BIORTECH.2018.06.113.

Publisher's Note